An objective definition of a vortex

By G. HALLER

Department of Mechanical Engineering, Massachusetts Institute of Technology,
77 Massachusetts Avenue, Rm 3-352, Cambridge, MA 02139, USA
ghaller@mit.edu

The most widely used definitions of a vortex are not objective: they identify different structures as vortices in frames that rotate relative to each other. Yet a frame-independent vortex definition is essential for rotating flows and for flows with interacting vortices. Here we define a vortex as a set of fluid trajectories along which the strain acceleration tensor is indefinite over directions of zero strain. Physically, this objective criterion identifies vortices as material tubes in which material elements do not align with directions suggested by the strain eigenvectors. We show using examples how this vortex criterion outperforms earlier frame-dependent criteria. As a side result, we also obtain an objective criterion for hyperbolic Lagrangian structures.

1. Introduction

The notion of a *vortex* is so widely used in fluid dynamics that few pause to examine what the word strictly means. Those who do take a closer look quickly realize the difficulty of defining vortices unambiguously.

Vortices are often thought of as regions of high vorticity, but there is no universal threshold over which vorticity is to be considered high. More alarmingly, vorticity may also be high in parallel shear flows where no vortices are present.

Definitions requiring closed or spiralling streamlines for a vortex are also ambiguous, because streamline topology changes even under simple Galilean transformations such as constant speed translations. Other definitions postulating pressure minima at vortex centres are readily refutable by counterexamples. Problems with all these definitions have been exposed by several authors, including Lugt (1979), Jeong & Hussain (1995), and Cucitore, Quadrio & Baron (1999).

1.1. *Galilean invariant vortex definitions*

Jeong & Hussain (1995) stress the need for Galilean-invariant vortex criteria, i.e. criteria that remain invariant under coordinate changes of the form $y = Qx + at$, where Q is a proper orthogonal tensor and a is a constant velocity vector. For a three-dimensional smooth velocity field $v(x, t)$, available Galilean-invariant vortex criteria use the velocity gradient decomposition

$$\nabla v = S + \Omega, \tag{1.1}$$

where $S = \frac{1}{2}[\nabla v + (\nabla v)^T]$ is the rate-of-strain tensor, and $\Omega = \frac{1}{2}[\nabla v - (\nabla v)^T]$ is the vorticity tensor.

In historical order, the first three-dimensional vortex criterion using (1.1) is the *Q-criterion* of Hunt, Wray & Moin (1988) which defines a vortex as a spatial region
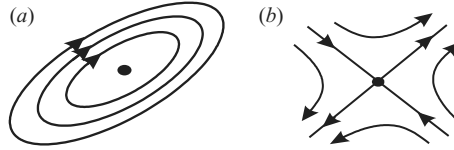
FIGURE 1. Instantaneous streamlines in a $z = $ const. plane for (a) the velocity field
(1.5), (b) the transformed velocity field (1.6).

where

$$Q = \frac{1}{2}[|\mathbf{\Omega}|^2 - |\mathbf{S}|^2] > 0, \tag{1.2}$$

i.e. where the Euclidean norm of the vorticity tensor dominates that of the rate of
strain. For two-dimensional flows, the same criterion has been known as the elliptic
version of the *Okubo–Weiss criterion*, derived independently by Okubo (1970) and
Weiss (1991). Hua & Klein (1998) and Hua, McWilliams & Klein (1998) propose a
higher-order correction to the Okubo–Weiss criterion by including acceleration terms.

Another well-known Galilean-invariant definition is the *Δ-criterion* of Chong,
Perry & Cantwell (1990), who define vortices as regions with

$$\Delta = \left(\frac{Q}{3}\right)^3 + \left(\frac{\det \nabla v}{2}\right)^2 > 0. \tag{1.3}$$

In these regions, the velocity gradient ∇v admits complex eigenvalues, thus local
instantaneous stirring is a plausible assumption.

Finally, according to the *λ_2-criterion* of Jeong & Hussain (1995), vortices are regions
where

$$\lambda_2(\mathbf{S}^2 + \mathbf{\Omega}^2) < 0, \tag{1.4}$$

where $\lambda_2(\mathbf{A})$ denotes the intermediate eigenvalue of a symmetric tensor $\mathbf{A}$. Under
appropriate adiabatic assumptions, this last criterion guarantees an instantaneous
local pressure minimum in a two-dimensional plane for Navier–Stokes flows.

1.2. *Is Galilean invariance enough?*

In an unsteady flow, as Lugt (1979) notes, there is no distinguished frame of reference.
An ideal vortex definition, therefore, should not depend on one's choice of frame.
Galilean-invariant criteria give consistent results in frames that move at constant
speeds relative to each other. The same criteria, however, fail to be invariant under
more general changes of frame such as rotations.

Consider, for instance, the linear velocity field

$$v(x, t) = \begin{pmatrix} \sin 4t & 2 + \cos 4t & 0 \\ -2 + \cos 4t & -\sin 4t & 0 \\ 0 & 0 & 0 \end{pmatrix} x, \tag{1.5}$$

whose instantaneous streamlines are sketched in figure 1(a). The criteria (1.2)–(1.4)
all predict that any point x lies in a *single infinite vortex*.

Now pass to the rotating frame

$$\tilde{x} = \begin{pmatrix} \cos 2t & \sin 2t & 0 \\ -\sin 2t & \cos 2t & 0 \\ 0 & 0 & 1 \end{pmatrix} x$$

to obtain the transformed velocity field

$$\tilde{\boldsymbol{v}}(\tilde{\boldsymbol{x}}) = \begin{pmatrix} 0 & 1 & 0 \\ 1 & 0 & 0 \\ 0 & 0 & 0 \end{pmatrix} \tilde{\boldsymbol{x}}. \tag{1.6}$$

The latter flow is a steady planar strain field (see figure 1*b*), in which the criteria (1.2)–(1.4) find *no vortices*. The discrepancy between the two results – an infinite vortex in one frame and no vortex in the other frame – is striking.

But why should vortex definitions give the same result in different rotating frames? Because in rotating flows and in flows with interacting vortices, there are several natural choices for a frame of reference: the lab frame, the frame co-rotating with the boundary, or the frames co-rotating with individual vortices. Obtaining different vortices in different frames from the same criterion is unsatisfactory at best, unphysical at worst.

Another related shortcoming of the Galilean-invariant criteria (1.2)–(1.4) is their direct dependence on the vorticity tensor $\boldsymbol{\Omega}$. As a result, these criteria will pronounce the whole fluid a single vortex in a fast enough rotating tank, missing all coherent structures in the flow.

1.3. *Objectivity*

In continuum mechanics, a quantity or principle is called *objective* if it remains invariant under coordinate changes of the form

$$\tilde{\boldsymbol{x}} = \boldsymbol{Q}(t)\boldsymbol{x} + \boldsymbol{b}(t), \tag{1.7}$$

where $\boldsymbol{Q}(t)$ is a time-dependent proper orthogonal tensor, and $\boldsymbol{b}(t)$ is a time-dependent translation vector (see Truesdell 1979 or Ottino 1989). Because (1.7) embodies all plausible changes of frame, we propose this notion of objectivity as a basic requirement for any consistent vortex definition.

Lugt (1979) takes an objective view when requiring a vortex to be a mass of fluid moving around a common axis. As indicators of such a Lagrangian vortex, he proposes closed or spiralling pathlines. Closed pathlines, however, are atypical even in steady three-dimensional flows, and the notion of spiralling pathlines is not objective.

Cucitore *et al.* (1999) describe vortices as material tubes of low particle dispersion. Relative dispersion as a diagnostic tool also appears in the earlier work of Elhmaïdi, Provenzale & Babiano (1993) on two-dimensional vortices. Such regions of low dispersion can also be inferred from finite-time Lyapunov-exponent studies (see, e.g., Pierrehumbert & Yang 1993). When formalized properly, dispersion-based vortex definitions are objective, but offer no connection between vortices and familiar physical quantities. In addition, low dispersion is also the hallmark of jets, and hence does not uniquely label vortices.

Tabor & Klapper (1994) offer a more systematic approach to vortices by studying the stability of fluid particles in the eigenbasis of the rate of strain $\boldsymbol{S}$. From this approach, they obtain a version of the Q-criterion in strain basis: they call a region rotation dominated if

$$Q_s = \frac{1}{2}[|\boldsymbol{\Omega} - \boldsymbol{\Omega}_s|^2 - |\boldsymbol{S}|^2] > 0, \tag{1.8}$$

where $\boldsymbol{\Omega}_s$ is a matrix containing the time derivatives of the unit eigenvectors of $\boldsymbol{S}$ in the Lagrangian frame. Lapeyre, Klein & Hua (1999) re-derive and test the same criterion for two-dimensional tracer gradient evolution. Lapeyre, Hua & Legras (2001)

discuss the advantages of using $Q_s < 0$, as opposed to $Q < 0$, in detecting regions of stretching in two-dimensional flows (see also Haller 2001*b*).

The Q_s-criterion is objective and can be turned into a mathematically exact vortex definition for two-dimensional flows. Specifically, fluid particles satisfying $Q_s > 0$ for long enough times are proven to form impenetrable swirling regions (Haller 2001*b* and Koh & Legras 2002). Unfortunately, as Tabor & Klapper (1995) note, the principle used in deriving (1.8) is two-dimensional, leaving the mathematical meaning of (1.8) unclear in three dimensions.

1.4. *Results*

In this paper, we describe vortices through the stability of fluid trajectories in three-dimensional incompressible flows. We first prove that a trajectory is hyperbolic (saddle-type) as long as the strain acceleration tensor

$$\boldsymbol{M} = \partial_t \boldsymbol{S} + (\nabla \boldsymbol{S})\boldsymbol{v} + \boldsymbol{S}(\nabla \boldsymbol{v}) + (\nabla \boldsymbol{v})^T \boldsymbol{S}$$

remains positive definite over a zero strain cone Z that travels with the trajectory. Hyperbolic trajectories form stable and unstable manifolds that are responsible for stretching, folding, and tracer filamentation in the flow.

Because $\boldsymbol{M}_Z$, the restriction of $\boldsymbol{M}$ to Z, turns out to be either positive definite or indefinite at a generic point, the above hyperbolicity result motivates us to define vortices as sets of fluid trajectories with indefinite $\boldsymbol{M}_Z$. Unlike previous vortex definitions, this $\boldsymbol{M}_Z$-criterion is objective, giving the same result in frames that translate or rotate relative to each other.

Physically, the $\boldsymbol{M}_Z$-criterion defines a vortex as a material region where material elements do not align with subspaces that are near the positive eigenspaces of the rate of strain. In other words, the long-term evolution of material elements defies the trend suggested by the instantaneous rate-of-strain tensor.

Our vortex definition is derived from Lagrangian considerations, but uses Eulerian quantities. This enables us to rewrite the $\boldsymbol{M}_Z$-criterion in terms of pressure and viscous terms for Navier–Stokes flows (see §5).

To test the $\boldsymbol{M}_Z$-criterion, we consider three-dimensional examples of rotating flows and interacting vortices. The examples include a steady Stokes flow (spherical drop flow), a steady Euler flow (ABC flow), and an unsteady flow (perturbation of the ABC flow). For all three examples, the $\boldsymbol{M}_Z$-criterion outperforms earlier vortex criteria.

2. Linearized velocity and the rate of strain

Consider a three-dimensional incompressible velocity field

$$\boldsymbol{v}(\boldsymbol{x}, t) = (u(x, y, z, t), v(x, y, z, t), w(x, y, z, t))^T, \qquad \nabla \cdot \boldsymbol{v} = 0,$$

with the corresponding fluid trajectories $\boldsymbol{x}(t)$ starting from $\boldsymbol{x}(t_0) = \boldsymbol{x}_0$ at time t_0. In the Lagrangian frame, an infinitesimal perturbation $\boldsymbol{\xi}$ to the initial condition $\boldsymbol{x}_0$ is advected by the linearized flow

$$\dot{\boldsymbol{\xi}} = \nabla \boldsymbol{v}\,(\boldsymbol{x}(t), t)\,\boldsymbol{\xi}, \tag{2.1}$$

the equation of variations associated with the trajectory $\boldsymbol{x}(t)$. The stability of the $\boldsymbol{\xi} = 0$ solution of (2.1) determines the linear stability of the underlying fluid trajectory.

To study the stability of $\boldsymbol{\xi} = 0$ in (2.1), we consider the Lyapunov function

$$V(\boldsymbol{\xi}, t) = \frac{1}{2}\frac{\mathrm{d}}{\mathrm{d}t}\,|\boldsymbol{\xi}|^2 = \langle \boldsymbol{\xi}, \boldsymbol{S}(\boldsymbol{x}(t), t)\boldsymbol{\xi} \rangle, \tag{2.2}$$
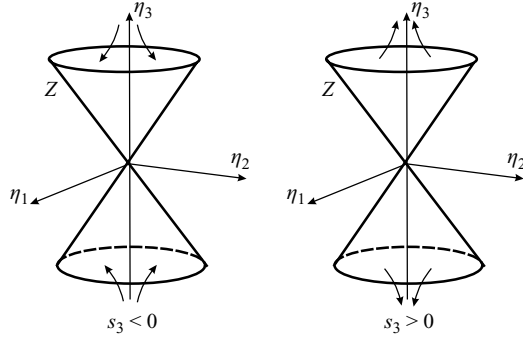
FIGURE 2. The elliptic cone Z in strain basis, and the behaviour of solutions inside Z
for $s_3 < 0$ and $s_3 > 0$.

where $\mathbf{S}(x, t)$ is the rate-of-strain tensor defined in (1.1). To exclude degenerate flows
from our discussion, we shall assume

$$\det \mathbf{S}(x, t) \neq 0 \tag{2.3}$$

throughout this paper. Two-dimensional flows violate this assumption, but they are
nonetheless amenable to a simplified version of the present approach (see Haller
2001*c*).

A negative value of V along a vector $\boldsymbol{\xi}$ implies instantaneous decay for $|\boldsymbol{\xi}|$, while
positive V values indicate growing $|\boldsymbol{\xi}|$. By incompressibility, the symmetric tensor $\mathbf{S}$
has zero trace, and hence out of its three eigenvalues, s_1, s_2, and s_3, at least one is
positive and at least one is negative. We index these eigenvalues so that

$$\text{sign } s_1 = \text{sign } s_2 \neq \text{sign } s_3, \qquad |s_1| \geqslant |s_2|, \tag{2.4}$$

thus s_1 and s_2 have the same sign.

3. Instantaneous Lagrangian flow geometry

By incompressibility and by (2.3), the tensor $\mathbf{S}$ is indefinite; the Lyapunov
function V, therefore, takes both positive and negative values in an arbitrary small
neighbourhood of $\boldsymbol{\xi} = 0$. The domains of positive and negative V values are separated
by the zero set

$$Z(x, t) = \{\boldsymbol{\xi} | \langle \boldsymbol{\xi}, \mathbf{S}(x, t)\boldsymbol{\xi} \rangle = 0\},$$

whose geometry is best understood in the basis of eigenvectors e_i corresponding to
the strain eigenvalues s_i.

Defining the coordinates (η_1, η_2, η_3) through

$$\boldsymbol{\xi} = \eta_1 e_1 + \eta_2 e_2 + \eta_3 e_3,$$

we find that Z satisfies

$$\eta_3^2 = a\eta_1^2 + (1 - a)\eta_2^2, \qquad a(x, t) = -\frac{s_1(x, t)}{s_3(x, t)} \in (0, 1), \tag{3.1}$$

which defines an elliptic cone in the strain basis, as shown in figure 2. Depending on
the sign of s_3, solutions of (2.1) that lie instantaneously inside Z approach the origin
($s_3 < 0$) or leave the origin ($s_3 > 0$).

The global geometry of solutions of (2.1) depends on how they cross the cone Z.
Because V has different signs inside and outside Z, the direction of crossing can be
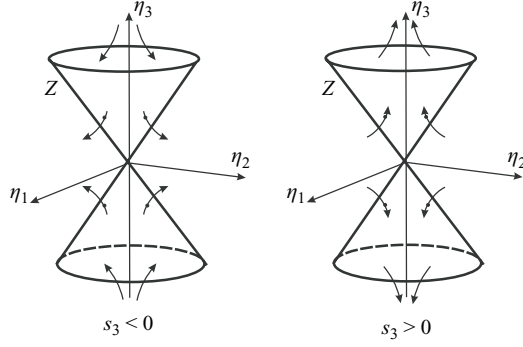
FIGURE 3. Instantaneous flow geometry near the trajectory (now at $\boldsymbol{\eta}=0$) when $\boldsymbol{M}$ is positive definite on Z. Dots on the trajectories refer to their point of entry (exit) into (out of) Z.
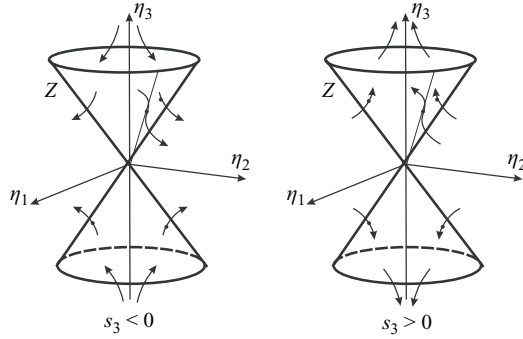

FIGURE 4. Same as figure 3 for the case when $\boldsymbol{M}$ is positive semidefinite on Z.

identified from the instantaneous growth or decay of V at the crossing point. Such growth or decay of V along solutions of (2.1) may be deduced from the derivative

$$\frac{\mathrm{d}}{\mathrm{d}t}V(\boldsymbol{\xi}(t),t) = \langle \boldsymbol{\xi}, \boldsymbol{M}(\boldsymbol{x}(t),t)\boldsymbol{\xi}\rangle \,,$$

where

$$\boldsymbol{M} = \dot{\boldsymbol{S}} + \boldsymbol{S}\,(\nabla\boldsymbol{v}) + (\nabla\boldsymbol{v})^{T}\,\boldsymbol{S} \tag{3.2}$$

denotes the *strain-acceleration tensor*, and $\dot{\boldsymbol{S}} = \partial_{t}\boldsymbol{S} + (\nabla\boldsymbol{S})\boldsymbol{v}$ denotes the material derivative of $\boldsymbol{S}$. Inflow or outflow through Z, therefore, depends on the sign of the quadratic form $\langle \boldsymbol{\xi}, \boldsymbol{M}\boldsymbol{\xi}\rangle$ on Z.

In continuum mechanics terms, $\boldsymbol{M}$ is an objective material derivative, the Cotter–Rivlin rate of $\boldsymbol{S}$ (see Cotter & Rivlin 1955). The trace of $\boldsymbol{M}$ is

$$\mathrm{Tr}\,\boldsymbol{M} = \mathrm{Tr}\,\dot{\boldsymbol{S}} + 2\,|\boldsymbol{S}|^{2} \,,$$

where $|\boldsymbol{S}| = \sqrt{\Sigma_{i,j}S_{ij}^{2}}$ denotes the Euclidean norm of $\boldsymbol{S}$. Because $\boldsymbol{S}$ has zero trace, we have $\mathrm{Tr}\,\dot{\boldsymbol{S}} = 0$, thus

$$\mathrm{Tr}\,\boldsymbol{M} = 2|\boldsymbol{S}|^{2} > 0 \tag{3.3}$$

holds for incompressible flows by assumption (2.3). Consequently, $\langle \boldsymbol{\xi}, \boldsymbol{M}\boldsymbol{\xi}\rangle$ is either positive definite, positive semidefinite, or indefinite over the cone Z. The corresponding instantaneous flow geometries are shown in figures 3–5.
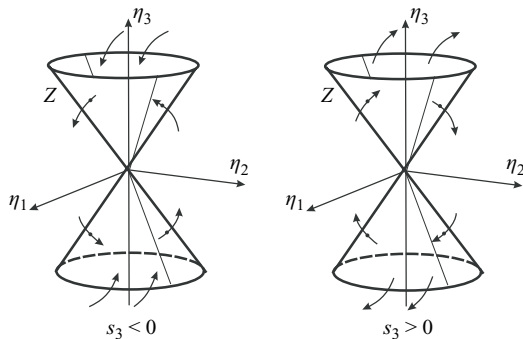
FIGURE 5. Same as figure 3 for the case when $\boldsymbol{M}$ is indefinite on Z.

The zero lines of $\langle \boldsymbol{\xi}, \boldsymbol{M}\boldsymbol{\xi} \rangle$ on Z are intersections of the zero-strain-acceleration cone

$$Z_{\boldsymbol{M}}(\boldsymbol{x}, t) = \{\boldsymbol{\xi} | \langle \boldsymbol{\xi}, \boldsymbol{M}(\boldsymbol{x}, t)\boldsymbol{\xi} \rangle = 0\}$$

with the zero-strain cone Z. Figures 4 and 5 show cases when Z consists of one and two such lines, respectively; three or four zero lines are also possible.

We call $\boldsymbol{M}$ *positive definite, positive semidefinite, or indefinite* on the cone Z if the quadratic form $\langle \boldsymbol{\xi}, \boldsymbol{M}\boldsymbol{\xi} \rangle$ is positive definite, positive semidefinite, or indefinite on Z. As shorthand notation, we shall use $\boldsymbol{M}_Z = \boldsymbol{M}|Z$ for the restriction of the tensor field $\boldsymbol{M}(\boldsymbol{x}, t)$ to the zero-strain cone field $Z(\boldsymbol{x}, t)$.

We note that Klein, Hua & Lapeyre (2000) derived a scalar multiple of the tensor $\boldsymbol{M}$ in studying passive tracer evolution in two-dimensional turbulence. They found that the eigenvectors of that tensor govern tracer gradient alignment in certain regions of the flow.

4. Hyperbolicity, ellipticity and vortices: an objective view

What can we infer from the instantaneous flow geometries of figures 3–5 about the stability of the trajectory $\boldsymbol{x}(t)$? This question is non-trivial to answer for two reasons. First, the equation of variations is a time-dependent linear ODE, and hence instantaneous features of its right-hand side (such as eigenvalues) are unrelated to the true asymptotics of its solutions (see e.g. Verhulst 1990). Second, the linear stability type of the origin $\boldsymbol{\xi} = 0$ may only reflect the linear stability of the trajectory $\boldsymbol{x}(t)$, and not its actual nonlinear stability.

Using dynamical systems techniques, we shall overcome the above difficulties for trajectories of saddle-type stability. The result is a sufficient criterion (Theorem 1) that guarantees saddle-type behaviour in the Lagrangian frame as long as the trajectory remains in an appropriately defined hyperbolic domain of the Eulerian frame. We then define vortices as sets of trajectories that remain in the complement of this Eulerian hyperbolic domain.

To state Theorem 1, we use an objective partition of the three-dimensional space into hyperbolic and elliptic domains. The *hyperbolic domain* $\mathcal{H}(t)$ is the set of $\boldsymbol{x}$ points at which $\boldsymbol{M}_Z$ is positive definite. We further partition the domain $\mathcal{H}(t)$ into two subdomains by letting

$$\mathcal{H}(t) = \mathcal{H}^-(t) \cup \mathcal{H}^+(t),$$

with the subscript of each subdomain referring to the sign of $s_3(\boldsymbol{x}, t)$ in that subdomain.

The *elliptic domain* $\mathscr{E}(t)$ is the set of $\boldsymbol{x}$ points at which $\boldsymbol{M}_Z$ is indefinite. The hyperbolic and elliptic domains are typically three-dimensional open sets separated by two-dimensional boundaries. One may call the union of all these boundaries the *parabolic domain* $\mathscr{P}(t)$.

4.1. *Lagrangian hyperbolicity from Eulerian quantities*

Lagrangian hyperbolicity (saddle-type behaviour) is the stability type of trajectories in regions of sustained material stretching and folding. In the language of nonlinear dynamics, these trajectories form stable and unstable manifolds that drive advective mixing in the fluid. Below we give a result that relates Lagrangian hyperbolicity to the Eulerian hyperbolic domain $\mathscr{H}(t)$.

THEOREM 1. *Fluid trajectories staying in the domain $\mathscr{H}^-(t)$ or $\mathscr{H}^+(t)$ are Lagrangian-hyperbolic. More specifically:*

(i) *For any fluid trajectory that stays in $\mathscr{H}^-(t)$, there is a one-dimensional material curve $\mathscr{S}(t)$ of fluid particles that converge to the trajectory while it stays in $\mathscr{H}^-(t)$. At the same time, there is a two-dimensional material surface $\mathscr{U}(t)$ of fluid particles that converge to the trajectory in backward time while it stays in $\mathscr{H}^-(t)$.*

(ii) *For any fluid trajectory that stays in $\mathscr{H}^+(t)$, there is a two-dimensional material surface $\mathscr{S}(t)$ of fluid particles that converge to the trajectory while it stays in $\mathscr{H}^+(t)$. At the same time, there is a one-dimensional material curve $\mathscr{U}(t)$ of fluid particles that converge to the trajectory in backward time while it stays in $\mathscr{H}^+(t)$.*

We prove the above theorem in Appendix C.

Theorem 1 implies that along trajectories staying in the hyperbolic region $\mathscr{H}(t)$, material elements align with time-varying subspaces that are close to the eigenvectors or eigenplanes of positive strain ($V > 0$). Thus, in hyperbolic regions, long-term material alignment conforms to what is suggested by the eigenvalue configuration of the rate of strain.

To apply Theorem 1, we need to evaluate the definiteness of the tensor $\boldsymbol{M}$ along the cone field Z, a costly undertaking at first sight. The following result of Appendix A, however, brings considerable simplification: $\boldsymbol{M}_Z$ is positive definite if and only if the quartic equation

$$p^4 + Ap^3 + Bp^2 + Cp + D = 0, \tag{4.1}$$

with its coefficients defined in (A 7), has no zeros in the $[-1, 1]$ interval. The coefficients A, B, C and D only depend on $\boldsymbol{M}$ and $\boldsymbol{S}$, and hence are objective.

The positive definiteness of $\boldsymbol{M}_Z$ also follows if $\boldsymbol{M}$ is a positive-definite tensor, which is the case if and only if

$$(4|\boldsymbol{S}|^4 - |\boldsymbol{M}|^2)|\boldsymbol{S}|^2 > \det \boldsymbol{M} > 0, \tag{4.2}$$

as we show in Appendix B. A positive definite $\boldsymbol{M}$ forces solutions of (2.1) to cross all level surfaces of the Lyapunov function V from lower towards higher values. This leads to *strong hyperbolicity*, a more uniform saddle-type behaviour compared to the case when $\boldsymbol{M}$ is only positive definite on Z.

Under certain conditions, Lagrangian hyperbolicity can also be inferred rigorously from the Lagrangian version of the Q-criterion (Haller 2001*a*). This latter approach, however, is not objective, and assumes the velocity field to be slowly varying.

4.2. *An objective vortex definition*

Motivated by our Lagrangian hyperbolicity result in Theorem 1, we define a vortex to be a bounded and connected set of fluid trajectories that remain in the elliptic
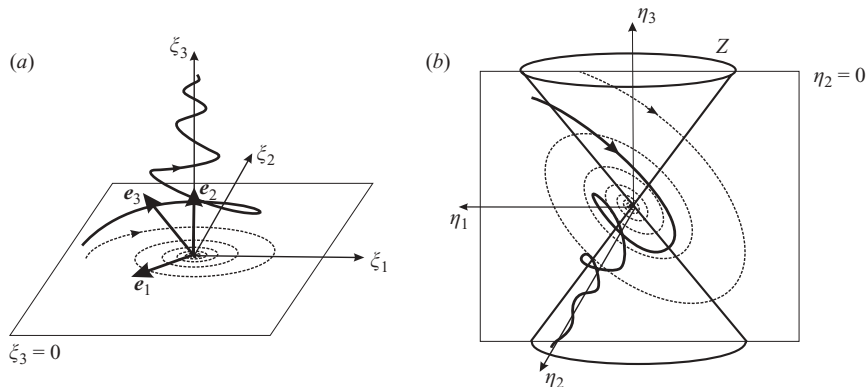
FIGURE 6. The linearized flow generated by the velocity gradient (4.3): (*a*) in the original basis (*b*) in strain basis.

region $\mathscr{E}(t)$, thereby avoiding the hyperbolic domain $\mathscr{H}(t)$. Equivalently, *a vortex is a set of fluid trajectories along which $\boldsymbol{M}_Z$ is indefinite.* We shall refer to this definition as the $\boldsymbol{M}_Z$-*criterion*.

By Theorem 1, the above definition identifies a vortex as a set of fluid trajectories along which material surface elements do not align with subspaces near the eigenspaces of positive strain. This is because in the elliptic domain $\mathscr{E}(t)$, there are always solutions of (2.1) that cross from the positive ($V > 0$) side of the zero-strain cone Z to the negative ($V > 0$) side. As a result, material alignment is either absent or inconsistent with the trend suggested by the eigenvalues of the rate of strain.

On a more qualitative note, the $\boldsymbol{M}_Z$-criterion identifies vortices as regions of objective *Lagrangian stirring*. By contrast, the Galilean-invariant definitions surveyed earlier identify vortices as regions of instantaneous Eulerian stirring, a feature inferred from non-objective quantities.

As a kinematic example, let us consider a fluid trajectory $\boldsymbol{x}(t)$, along which the linearized flow $\dot{\boldsymbol{\xi}} = \nabla \boldsymbol{v}(\boldsymbol{x}(t), t)\boldsymbol{\xi}$ admits the constant velocity gradient

$$\nabla \boldsymbol{v}(\boldsymbol{x}(t), t) = \begin{pmatrix} -1 & 9 & 0 \\ -1 & -1 & 0 \\ 0 & 0 & 2 \end{pmatrix}. \tag{4.3}$$

This linearized flow produces a tornado-type vortex with inward spiralling parallel to the (ξ_1, ξ_2)-plane and stretching along the ξ_3-axis (see figure 6a).

With the ordering (2.4), the strain eigenvalues for the above vortex are

$$s_1 = 3, \quad s_2 = 2, \quad s_3 = -5,$$

with the corresponding strain eigenvectors

$$\boldsymbol{e}_1 = \begin{pmatrix} -\sqrt{2}/2 \\ -\sqrt{2}/2 \\ 0 \end{pmatrix}, \qquad \boldsymbol{e}_2 = \begin{pmatrix} 0 \\ 0 \\ 1 \end{pmatrix}, \qquad \boldsymbol{e}_3 = \begin{pmatrix} -\sqrt{2}/2 \\ \sqrt{2}/2 \\ 0 \end{pmatrix}.$$

Figure 6(*b*) shows the trajectories of the linearized flow in strain basis. Note that trajectories near the invariant plane $\eta_2 = 0$ ($\xi_3 = 0$) enter and leave the zero-strain cone Z repeatedly before aligning with the intermediate strain axis $\boldsymbol{e}_2$. The quadratic form

$V(\boldsymbol{\xi})$ and the strain acceleration tensor $\boldsymbol{M}$ are, therefore, indefinite on Z. Consequently, the underlying fluid trajectory $\boldsymbol{x}(t)$ is contained in a vortex by the $\boldsymbol{M}_Z$-criterion.

5. Hyperbolicity and vortices in Navier–Stokes flows

Along a trajectory $\boldsymbol{x}(t)$ generated by a Navier–Stokes velocity field, the rate of strain $\boldsymbol{S}$ satisfies the differential equation

$$\dot{\boldsymbol{S}} = -(\boldsymbol{S}^2 + \boldsymbol{\Omega}^2) - \frac{1}{\rho}\boldsymbol{P} + \nu\Delta\boldsymbol{S}, \tag{5.1}$$

where $\boldsymbol{\Omega}$ is the vorticity tensor defined in (1.1), and $P_{ij} = \partial^2 p/\partial x_i \partial x_j$ is the pressure Hessian (see Tabor & Klapper 1994 and Jeong & Hussein 1995). Substituting (5.1) into (3.2) yields

$$\boldsymbol{M} = (\boldsymbol{S} - \boldsymbol{\Omega})(\nabla \boldsymbol{v}) + \nu\Delta\boldsymbol{S} - \frac{1}{\rho}\boldsymbol{P}, \tag{5.2}$$

whose restriction to the zero-strain cone field is

$$\left[(\boldsymbol{S} - \boldsymbol{\Omega})(\nabla \boldsymbol{v}) + \nu\Delta\boldsymbol{S} - \frac{1}{\rho}\boldsymbol{P}\right]_Z. \tag{5.3}$$

Thus, for Navier–Stokes flows, trajectories on which the tensor (5.3) is positive definite form hyperbolic material lines and surfaces (stable and unstable manifolds). Accordingly, our vortex definition for three-dimensional Navier–Stokes flows can be phrased as follows: *A vortex is a set of fluid trajectories along which the tensor* (5.3) *is indefinite.*

Replacing the kinematic formula for $\boldsymbol{M}$ (4.2) with (5.2), we find that strong hyperbolicity holds over regions where

$$4|\boldsymbol{S}|^4 - \text{Tr}\left[(\boldsymbol{S} - \boldsymbol{\Omega})(\nabla\boldsymbol{v}) + \nu\Delta\boldsymbol{S} - \frac{1}{\rho}\boldsymbol{P}\right]^2 > \frac{\det\left[(\boldsymbol{S} - \boldsymbol{\Omega})(\nabla\boldsymbol{v}) + \nu\Delta\boldsymbol{S} - \frac{1}{\rho}\boldsymbol{P}\right]}{|\boldsymbol{S}|^2} > 0. \tag{5.4}$$

As opposed to our earlier kinematic formulae, the dynamic formulae (5.3) and (5.4) contain no time derivatives. Thus (5.3) and (5.4) extend to velocity fields that are non-differentiable in time, as long as they are twice continuously differentiable in space. To obtain similar expressions for hyperbolic and elliptic domains in Euler flows, one simply sets $\nu = 0$ in (5.3) and (5.4).

6. Numerical examples

In this paper, we consider three analytic velocity fields of increasing complexity to illustrate the use of the $\boldsymbol{M}_Z$-criterion. All three examples involve rotating frames or interacting vortices.

To compare the $\boldsymbol{M}_Z$-criterion to other vortex criteria, we use finite-time Lyapunov exponent distributions as objective benchmarks. KAM-type regions of low particle dispersion show up as domains of minima for Lyapunov exponents. Such regions are arguably considered vortices in agreement with Elhmaïdi *et al.* (1993) and Cucitore *et al.* (1999). Still, we prefer not to define vortices via Lyapunov exponents, because (i) these exponents have no direct relation to Eulerian features of the velocity field (ii) Lyapunov exponents also admit low values in parallel shear flows with no vortices.

Two remarks are in order about the numerical implementation of the $\boldsymbol{M}_Z$-criterion. First, significant numerical errors may accumulate from long-term trajectory

integration, and from the second-order numerical differentiation involved in computing $\boldsymbol{M}$ and Z. As a result, the computation will erroneously place some fluid particles outside $\mathscr{E}(t)$, even if they are actually inside $\mathscr{E}(t)$. No matter how short, such an excursion would disqualify the trajectory from being in a vortex. In a fluid flow with Lagrangian chaos, most trajectories will temporarily leave a vortex for this reason.

To address the above computational difficulty, we employ a numerically more robust version of the $\boldsymbol{M}_Z$-criterion: a vortex is a set of fluid trajectories along which $\boldsymbol{M}_Z$ is indefinite for longer times than along nearby trajectories. In other words, we require the time of indefiniteness of $\boldsymbol{M}_Z$ to admit a local maximum over trajectories contained in a vortex. This relaxed definition allows for short excursions outside $\mathscr{E}(t)$.

Second, while the number of zeros of equation (4.1) can be determined analytically by Sturm's theorem (Barbeau 1989), we prefer to use an equivalent result for the definiteness of $\boldsymbol{M}_Z$ from Appendix A. Specifically, $\boldsymbol{M}_Z$ is positive definite if and only if the quantity $m(\alpha)$ defined in (A 2) is positive for all $\alpha \in [0, 2\pi]$. Testing the sign of $m(\alpha)$ over $[0, 2\pi]$ is simpler than computing the quantities appearing in Sturm's theorem.

6.1. *Spherical drop in a Stokes flow*

Stone, Nadim & Strogatz (1991) showed that in the Stokes limit, the velocity field of a spherical drop immersed in an external strain field takes the form

$$
\left.
\begin{aligned}
u(\boldsymbol{x}) &= \frac{1}{2}\left[(5|\boldsymbol{x}|^2 - 3)\frac{x}{1+a} - 2x\left(\frac{x^2}{1+a} + \frac{ay^2}{1+a} - z^2\right)\right] + \frac{1}{2}(\omega_y z - \omega_z y), \\
v(\boldsymbol{x}) &= \frac{1}{2}\left[(5|\boldsymbol{x}|^2 - 3)\frac{ay}{1+a} - 2y\left(\frac{x^2}{1+a} + \frac{ay^2}{1+a} - z^2\right)\right] + \frac{1}{2}(\omega_z x - \omega_x z), \\
w(\boldsymbol{x}) &= \frac{1}{2}\left[-(5|\boldsymbol{x}|^2 - 3)z - 2z\left(\frac{x^2}{1+a} + \frac{ay^2}{1+a} - z^2\right)\right] + \frac{1}{2}(\omega_x y - \omega_y x).
\end{aligned}
\right\} \quad (6.1)
$$

Here a is the ratio of the first two eigenvalues of the rate of strain of the linear background flow, and $\boldsymbol{\omega} = (\omega_x, \omega_y, \omega_z)$ is the angular velocity vector of the drop. Stone *et al.* showed that the particle motion generated by (6.1) is integrable for $\omega_x = \omega_y = 0$, and is typically chaotic otherwise. Here we shall study vortices in the integrable limit to illustrate that frame invariance of vortex extraction is a crucial requirement even in that limit.

For $\boldsymbol{\omega} = 0$, as Stone *et al.* (1991) discuss, the drop stands still with a vortex ring in each of its hemispheres. These upper and lower vortices correspond to low values of the finite-time Lyapunov exponents shown in figure 7(*a*). The high values of the exponents mark the two-dimensional stable manifold of the origin in the (x, y)-plane, and the one-dimensional unstable manifold of the origin in the z-axis. Lighter colours in this figure mark regions of small dispersion.

Figure 7(*b–e*) shows the vortices obtained from the Δ-, λ_2-, Q-, and Q_s-criteria for $\boldsymbol{\omega} = 0$. All four criteria succeed in giving the rough location of the four intersections of the upper and lower vortex rings with the (y, z)-plane. The best result, however, is figure 7(*f*), the numerical implementation of the $\boldsymbol{M}_Z$-criterion. Here larger times spent in the elliptic region $\mathscr{E}$ correspond to darker colours; initial conditions remaining in $\mathscr{E}$ over the whole simulation interval $[0, 10]$ are coloured black. Note how the $\boldsymbol{M}_Z$-criterion captures the vortices the most faithfully, correctly reproducing their confinement to the interior of the spherical drop.
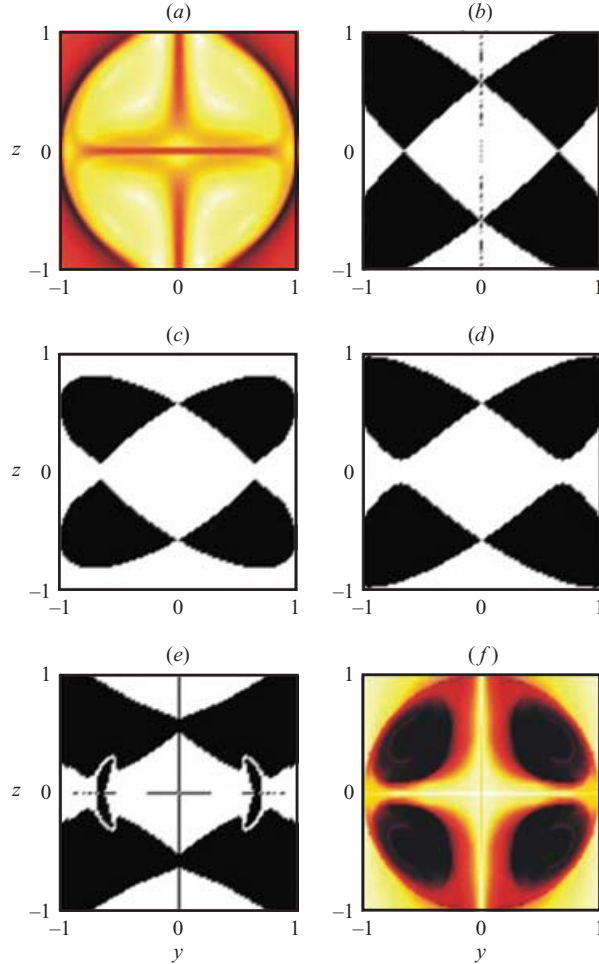
FIGURE 7. Evaluation of different vortex criteria on the (y, z)-plane of the spherical drop flow with $\boldsymbol{\omega} = 0$ and $a = 1$. (*a*) Finite-time Lyapunov exponents over the time interval $[0, 10]$, with darker colours indicating higher values. (*b*) $\Delta > 0$ (black region). (*c*) $\lambda_2 < 0$ (black region). (*d*) $Q > 0$ (black region). (*e*) $Q_s > 0$ (black region). (*f*) Time spent in the domain where $\boldsymbol{M}_Z$ is indefinite, with darker colours indicating longer times.

To consider the case of a rotating drop, we now set $\omega_x = \omega_y = 0$ and $\omega_z = 3$. This change in $\boldsymbol{\omega}$ is not a change of frame, because it leaves the background strain field unaffected. As a result, fluid trajectories change, even though the flow geometry remains qualitatively similar (see figure 8*a*). Figure 8(*b–d*) shows how the the Δ-, λ_2-, and Q- criteria fail to capture vortices: two of them even suggest that every point in the physical space is part of a single vortex. This illustrates our earlier point that in rotating flows, frame-dependent criteria will view the whole space as a single vortex if the speed of rotation is high enough.

The Q_s-criterion in figure 8(*e*) still indicates bounded vortex regions, but fails to capture the basic shape and location of vortex rings. By contrast, the $\boldsymbol{M}_Z$-criterion evaluated in figure 8(*f*) gives the correct vortex locations and physically reasonable vortex shapes.
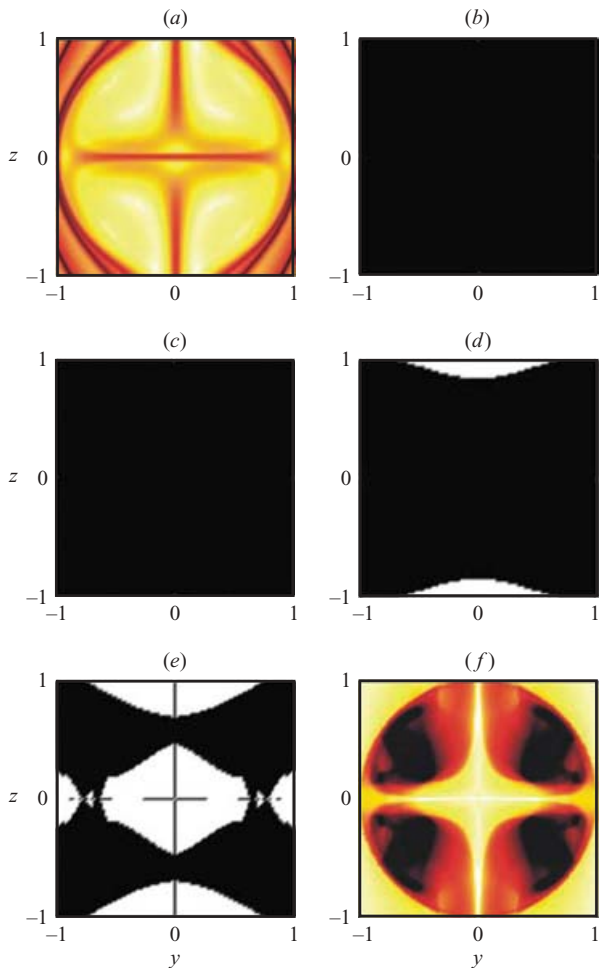
FIGURE 8. Same as figure 7, but with $\boldsymbol{\omega} = (0, 0, 3)$.

6.2. *ABC flow*

The classic ABC flow is given by the velocity field

$$\left.\begin{aligned}
u(\boldsymbol{x}) &= A \sin z + C \cos y, \\
v(\boldsymbol{x}) &= B \sin x + A \cos z, \\
w(\boldsymbol{x}) &= C \sin y + B \cos x,
\end{aligned}\right\} \tag{6.2}$$

which we consider with the parameter values $A = \sqrt{3}$, $B = \sqrt{2}$, and $C = 1$. This parameter configuration generates chaotic streamlines as described by Dombre *et al.* (1986), providing a more complex flow than the integrable Stokes example considered in §6.1.

The ABC flow is known to have KAM-type elliptic regions that are arguably called vortices, as they display swirling particle behaviour and small dispersion values. These regions have different sizes and spatial orientations, as the finite-time Lyapunov exponent distribution in the $x = 2\pi$ plane reveals (see figure 9a).

The black regions in figure 9(b–e) mark points of the $x = 2\pi$ plane where the Δ-criterion, the λ_2-criterion, the Q-criterion, and the Q_s-criterion are satisfied. These
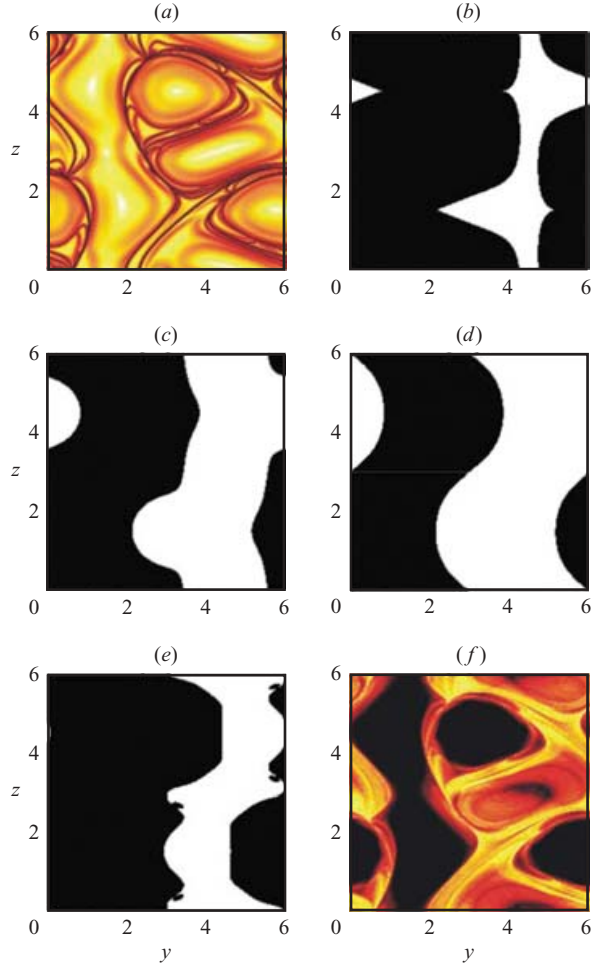
FIGURE 9. Visualization of the intersection of vortices with the $x = 2\pi$ plane in the ABC flow. (*a*) Finite-time Lyapunov exponents over the time interval [0, 10], with darker colours indicating higher values. (*b*) $\Delta > 0$ (black region). (*c*) $\lambda_2 < 0$ (black region). (*d*) $Q > 0$ (black region). (*e*) $Q_s > 0$ (black region). (*f*) Time spent in the domain where $\boldsymbol{M}_Z$ is indefinite, with darker colours indicating larger times; if the time is the entire simulation interval [0, 10], the trajectory is coloured black.

criteria all miss most vortices indicated by figure 9(*a*), with the exception of the single vortex that extends in the vertical direction of the left half of figure 9(*a*). The basic shape of this vortex, however, is incorrectly predicted by all these criteria: they all fail to capture how the vortex first bends to the right and then to the left for increasing z values.

By contrast, figure 9(*f*) shows the numerical implementation of the $\boldsymbol{M}_Z$-criterion. Note the close correlation between the black regions of this figure and the regions of low particle dispersion in figure 9(*a*). Specifically, out of the five vortices visible in 9(*a*), four are captured unambiguously by the $\boldsymbol{M}_Z$-criterion. The fifth vortex, with its centre located approximately at $(y, z) = (4.5, 3)$, is also recognizable in figure 9(*f*), but its core is blurred. The quality of this core improves if one marks all trajectories black that spend 90% of their time in the elliptic region (see figure 10.)
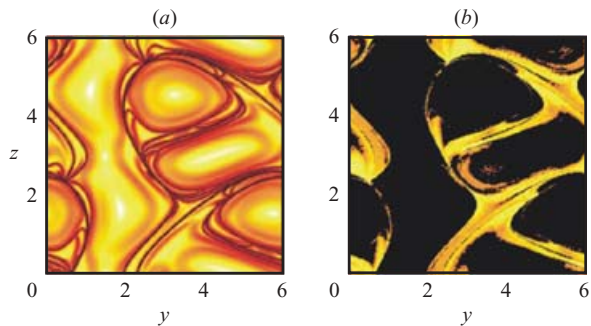
FIGURE 10. Visualization of the intersection of vortices with the $x = 2\pi$ plane in the ABC flow. (*a*) Finite-time Lyapunov exponents over the time interval [0, 10], with darker colours indicating higher values. (*b*) Time spent in the domain where $\boldsymbol{M}_Z$ is indefinite; if the time is at least 90% of the entire simulation interval [0, 10], the trajectory is coloured black.
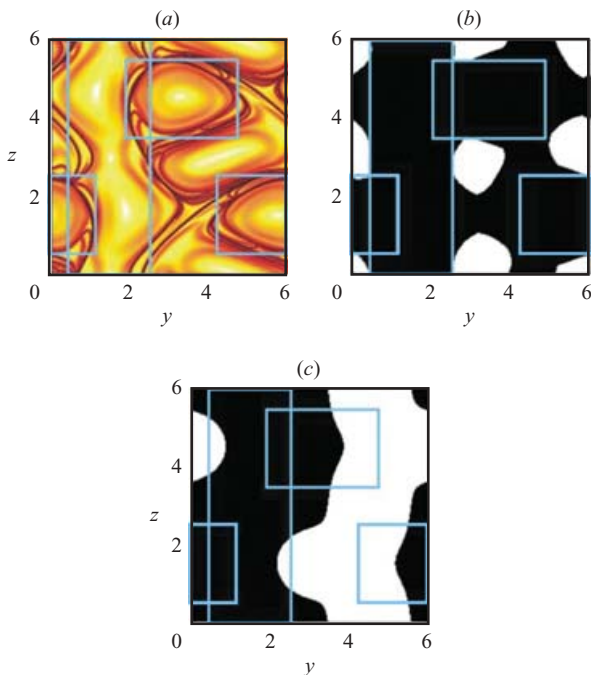

FIGURE 11. The rough location of vortices (marked by rectangles) as inferred from the Lyapunov exponent plot (*a*), then superimposed on the elliptic region shown in (*b*), and on the $\lambda_2 < 0$ region shown in (*c*).

While figure 9(*f*) reveals trajectories that stay in the elliptic domain $\mathscr{E}$, figure 11(*b*) shows fluid particles on the $x = 2\pi$ plane that are instantaneously in $\mathscr{E}$. Interestingly, the latter figure already suggests the rough location of some of the vortices, as the rectangles marking the approximate vortex locations confirm. For comparison, the reader may wish to consider the same rectangles superimposed on the vortex candidates provided by, say, the λ_2-criterion (see figure 11*c*).

Figure 12 gives a three-dimensional comparison of the vortex candidates obtained from different criteria. As seen in the figure, the objective vortex criterion (figure 12*f*)
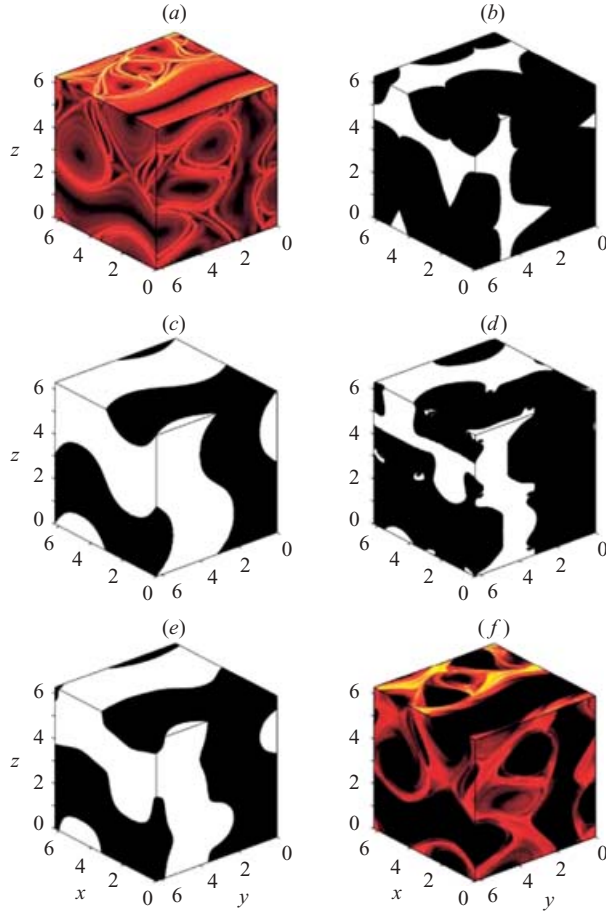
FIGURE 12. Evaluation of different vortex criteria on the faces of the $[0, 2\pi]^3$ cube in the ABC flow. (a) Finite-time Lyapunov exponents over the time interval $[0, 10]$, with darker colours indicating higher values. (b) $\Delta > 0$ (black region). (c) $Q > 0$ (black region). (d) $Q_s > 0$ (black region). (e) $\lambda_2 < 0$ (black region). (f) Time spent in the domain where $\boldsymbol{M}_Z$ is indefinite, with darker colours indicating larger times.

proposed in this paper provides the closest match for the vortices revealed by Lyapunov exponents.

Finally, figure 13 compares the three-dimensional Lyapunov exponent distribution with the elliptic set $\mathscr{E}$ shown in black. This comparison confirms that $\mathscr{E}$ itself already serves as a rough approximation for some of the vortices in the ABC flow.

6.3. Unsteady ABC-type flow

The ABC flow is an unstable solution of Euler's equation, displaying high-frequency instabilities under perturbation (see Friedlander & Vishik 1991 and Lifschitz 1991). To model these instabilities, we consider the unsteady velocity field

$$u(\boldsymbol{x}, t) = A(t) \sin z + C \cos y,$$
$$v(\boldsymbol{x}, t) = B \sin x + A(t) \cos z,$$
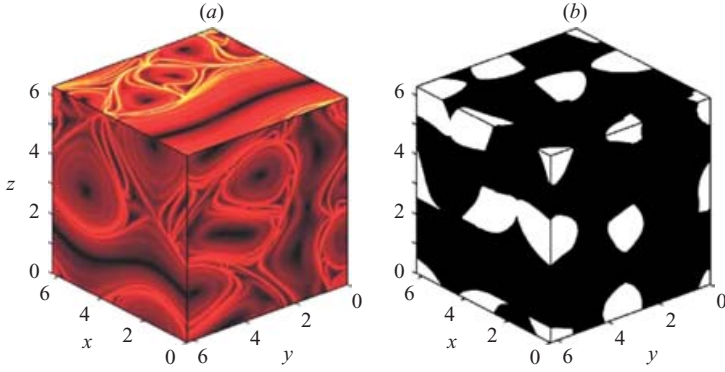$$w(\boldsymbol{x}, t) = C \sin y + B \cos x,$$

FIGURE 13. (*a*) Finite-time Lyapunov exponents (with lighter colours indicating larger values) and (*b*) the elliptic set $\mathscr{E}$ for the ABC flow.
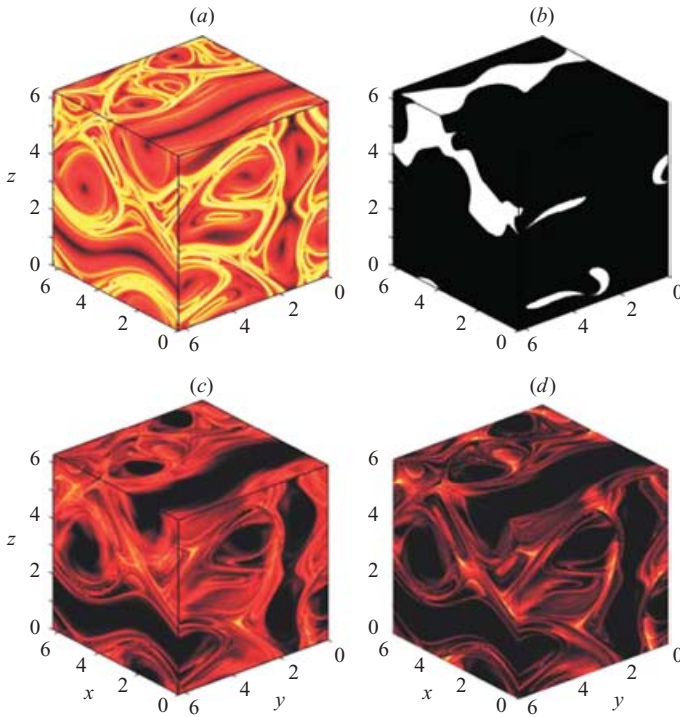

FIGURE 14. Evaluation of different vortex criteria on the faces of the $[0, 2\pi]^3$ cube in the unsteady ABC-type flow. (*a*) Finite-time Lyapunov exponents over the time interval $[0, 10]$, with darker colours indicating higher values. (*b*) $Q_s > 0$ (black region). (*c*) Time spent in the region where $\boldsymbol{M}_Z$ is indefinite, with darker colours indicating larger times. (*d*) Time spent in the domain where $\boldsymbol{M}$ is *not* positive definite, with darker colours indicating longer times.

where $A(t) = A_0 + (1 - e^{-qt}) \sin \omega t$ represents the effect of a growing and saturating unstable mode. This third example, therefore, adds unsteadiness to the already complex flow geometry of our second example.

For $A_0 = \sqrt{3}$, $q = 0.1$, $\omega = 2\pi$, $B = \sqrt{2}$, and $C = 1$, we again compare results from different vortex definitions using the Lyapunov exponent calculation of figure 14(*a*)

as an objective Lagrangian benchmark. For $t = 0$, the results from the Δ-criterion, the Q-criterion, and the λ_2-criterion are the same as in the steady case (see figure 12b, c, e), and are omitted here. While the Q_s-criterion (figure 14b) fails to capture any of the vortices indicated by Lyapunov exponents, the $\boldsymbol{M}_Z$-criterion (figure 14c) does identify these vortices accurately.

For the present example, we also plot trajectories along which $\boldsymbol{M}$ is not positive definite for long times. Shown in figure 14(d), these are the trajectories that consistently violate the inequalities (4.2), or in other words, stay away from the domain of strong hyperbolicity. The vortices emerging from this relaxed vortex definition ($\boldsymbol{M}$-criterion) are even sharper than those in figure 14(c). The performance of the $\boldsymbol{M}$-criterion, however, is problem dependent: Haller (2001c) gives an example in which the two-dimensional version of the $\boldsymbol{M}$-criterion gives weaker results than the two-dimensional $\boldsymbol{M}_Z$-criterion.

7. Conclusions

In this paper, we propose an objective vortex definition for three-dimensional incompressible flows. We first proved that a given fluid trajectory is hyperbolic in a strict mathematical sense as long as $\boldsymbol{M}$, the Cotter–Rivlin derivative of the rate of strain, is positive definite along the zero set Z of the quadratic form $\langle \boldsymbol{\xi}, \boldsymbol{S}\boldsymbol{\xi} \rangle$. By hyperbolicity, we mean a saddle-type instability in the Lagrangian frame that leads to exponential stretching and folding of nearby material surfaces. Our hyperbolicity criterion is objective, because both $\boldsymbol{M}$ and Z are objective.

For incompressible flows, $\boldsymbol{M}$ may only be positive definite, indefinite, or positive semidefinite on Z, with the latter case occurring on the boundary of hyperbolic regions. This prompted us to define vortices as sets of fluid trajectories along which $\boldsymbol{M}$ is indefinite on Z, or, for short, $\boldsymbol{M}_Z$ is indefinite.

For two-dimensional flows, our $\boldsymbol{M}_Z$-criterion simplifies to the Lagrangian version of the Q_s-criterion described in Haller (2001c). For three-dimensional flows, however, the $\boldsymbol{M}_Z$-criterion has no such relation to the Q_s-criterion; figures 12(d) and 13(b) show the difference between instantaneous evaluations of the two criteria in a concrete example.

We tested the $\boldsymbol{M}_Z$-criterion in three examples that involved rotating frames, interacting vortices, and growing instabilities. In all three examples, the $\boldsymbol{M}_Z$-criterion revealed sharp vortices that coincided with those suggested by Lyapunov exponent plots. By contrast, prior vortex definitions, such as the Q-, Q_s-, Δ-, and λ_2-criteria, typically gave an incorrect indication of the location and shape of vortices.

As the $\boldsymbol{M}_Z$-criterion is based on Lagrangian stability considerations, it shows close correlation with regions of low particle dispersion. While such regions are best captured by low values of finite-time Lyapunov exponents, these exponents do not provide clues about Eulerian features of vortices. By contrast, the $\boldsymbol{M}_Z$-criterion is based on objective invariants of the velocity field, and hence yields a link between vortices and the governing equations (see § 5).

We believe that further work is necessary to explore the implementation of the $\boldsymbol{M}_Z$-criterion in direct numerical simulations of unsteady flows. One numerical difficulty is already apparent from the present work: because of numerical errors, $\boldsymbol{M}_Z$ may appear positive definite for short times even on trajectories inside vortices. A way around this difficulty is to define vortices, for numerical purposes, as trajectories that spend most of their time in the region where $\boldsymbol{M}_Z$ is indefinite. Testing of this principle in direct numerical simulations is currently underway and will be reported elsewhere.

Appendix A

Here we give a sufficient and necessary criterion for the positive definiteness of $\boldsymbol{M}$ on Z. Letting $\eta_1 = l_1 \cos \alpha$, $\eta_2 = l_2 \sin \alpha$ in (3.1), denoting $\boldsymbol{M}$ in strain basis by

$$\hat{\boldsymbol{M}} = [\boldsymbol{e}_1 \; \boldsymbol{e}_2 \; \boldsymbol{e}_3]^T \boldsymbol{M} \, [\boldsymbol{e}_1 \; \boldsymbol{e}_2 \; \boldsymbol{e}_3],$$

and substituting the expression (3.1) for η_3 into $\langle \boldsymbol{\eta}, \hat{\boldsymbol{M}} \boldsymbol{\eta} \rangle$ gives

$$
\begin{aligned}
m(\alpha) = {} & l_1^2 (\hat{M}_{11} + a\hat{M}_{33}) \cos^2 \alpha + l_2^2 (\hat{M}_{22} + (1-a)\hat{M}_{33}) \sin^2 \alpha \\
& + 2\sqrt{l_1^2 a \cos^2 \alpha + l_2^2 (1-a) \sin^2 \alpha} (l_1 \hat{M}_{13} \cos \alpha + l_2 \hat{M}_{23} \sin \alpha) \\
& + l_1 l_2 \hat{M}_{12} \sin 2\alpha,
\end{aligned}
\tag{A 1}
$$

the restriction of $\langle \boldsymbol{\eta}, \boldsymbol{M} \boldsymbol{\eta} \rangle$ to the ellipse

$$\left(l_1 \cos \alpha, \, l_2 \sin \alpha, \, \sqrt{l_1^2 a \cos^2 \alpha + l_2^2 (1-a) \sin^2 \alpha} \right)$$

on the upper half of the cone Z.

For $l_1 = \sqrt{1-a}$ and $l_2 = \sqrt{a}$, formula (A 1) takes the simpler form

$$
\begin{aligned}
m(\alpha) = {} & \hat{M}_{11} (1-a) \cos^2 \alpha + \hat{M}_{22} a \sin^2 \alpha + \hat{M}_{33} a(1-a) \\
& + \sqrt{a(1-a)} (2\hat{M}_{13} \sqrt{1-a} \cos \alpha + 2\hat{M}_{23} \sqrt{a} \sin \alpha + \hat{M}_{12} \sin 2\alpha).
\end{aligned}
\tag{A 2}
$$

The strict positivity of $m(\alpha)$ over the interval $[0, 2\pi]$ is, therefore, equivalent to the positive definiteness of $\boldsymbol{M}$ on Z. Note that $m(\alpha)$ cannot be strictly negative on $[0, 2\pi]$, because $\boldsymbol{M}$ cannot be negative definite on Z. Consequently, to establish the positive definiteness of $\boldsymbol{M}$, we need to guarantee that $m(\alpha)$ has no real zeros.

Rewriting (A 2) as

$$
\begin{aligned}
m(\alpha) = {} & [\hat{M}_{11}(1-a) - \hat{M}_{22} a] \cos^2 \alpha + \hat{M}_{12} \sqrt{a(1-a)} \sin 2\alpha \\
& + 2\hat{M}_{13} \sqrt{a}(1-a) \cos \alpha + 2\hat{M}_{23} a \sqrt{1-a} \sin \alpha + \hat{M}_{33} a(1-a) + \hat{M}_{22} a
\end{aligned}
$$

shows that zeros of $m(\alpha)$ satisfy the equation

$$
\begin{aligned}
\pm 2\sqrt{a(1-a)} & \sqrt{1 - \cos^2 \alpha} (\hat{M}_{12} \cos \alpha + \sqrt{a} \hat{M}_{23}) \\
& = -[\hat{M}_{11}(1-a) - \hat{M}_{22} a] \cos^2 \alpha - 2\hat{M}_{13} \sqrt{a}(1-a) \cos \alpha \\
& \quad - \hat{M}_{33} a(1-a) - \hat{M}_{22} a,
\end{aligned}
\tag{A 3}
$$

with the sign of the left-hand side given by the sign of $\sin \alpha$. Letting $p = \cos \alpha$ and taking the square of both sides, we obtain

$$
\begin{aligned}
4(1 - p^2) a(1-a)(\hat{M}_{12} p + \sqrt{a} \hat{M}_{23})^2 = {} & [(\hat{M}_{11}(1-a) - \hat{M}_{22} a) p^2 \\
& + 2\hat{M}_{13} \sqrt{a}(1-a) p + a(\hat{M}_{33}(1-a) + \hat{M}_{22})]^2,
\end{aligned}
\tag{A 4}
$$

where we have selected the positive sign for $1 - p^2$ to ensure that the norm of any real root of (A 4) is less than unity. As a result, any real root yields a corresponding zero for equation (A 3).

If

$$S_0 = [\hat{M}_{11}(1-a) - \hat{M}_{22}a]^2 + 4\hat{M}_{12}^2 a(1-a) \neq 0, \tag{A 5}$$

then equation (A 4) is equivalent to

$$p^4 + Ap^3 + Bp^2 + Cp + D = 0, \tag{A 6}$$

with

$$\left. \begin{aligned} A &= 4\sqrt{a}(1-a)\frac{\hat{M}_{13}[\hat{M}_{11}(1-a) - \hat{M}_{22}a] + 2a\hat{M}_{12}\hat{M}_{23}}{S_0}, \\ B &= 4a\frac{\hat{M}_{13}^2(1-a)^2 + (1-a)(a\hat{M}_{23}^2 - \hat{M}_{12}^2)}{S_0} \\ &\quad + 2a\frac{[\hat{M}_{11}(1-a) - \hat{M}_{22}a][\hat{M}_{33}(1-a) + \hat{M}_{22}]}{S_0}, \\ C &= 4\sqrt{a^3}(1-a)\frac{\hat{M}_{13}[\hat{M}_{33}(1-a) + \hat{M}_{22}] - 2\hat{M}_{12}\hat{M}_{23}}{S_0}, \\ D &= a^2\frac{[\hat{M}_{33}(1-a) + \hat{M}_{22}]^2 - 4(1-a)\hat{M}_{23}^2}{S_0}. \end{aligned} \right\} \tag{A 7}$$

Therefore, the tensor $\boldsymbol{M}$ is positive definite on the cone Z if and only if (A 6) has no real roots in the $[-1, 1]$ interval.

Appendix B

Here we derive formula (4.2) for the positive definiteness of the tensor $\boldsymbol{M}$. The characteristic equation of $\boldsymbol{M}$ is

$$\lambda^3 - \mathrm{Tr}\,\boldsymbol{M}\lambda^2 + I_2(\boldsymbol{M})\,\lambda - \det\boldsymbol{M} = 0,$$

where

$$I_2(\boldsymbol{M}) = \frac{1}{2}[(\mathrm{Tr}\,\boldsymbol{M})^2 - \mathrm{Tr}\,\boldsymbol{M}^2] \tag{B 1}$$

is the second scalar invariant of $\boldsymbol{M}$. We change to the new variable $\zeta = -\lambda$ to obtain the transformed characteristic equation

$$\zeta^3 + \mathrm{Tr}\,\boldsymbol{M}\zeta^2 + I_2(\boldsymbol{M})\,\zeta + \det\boldsymbol{M} = 0. \tag{B 2}$$

By the symmetry of $\boldsymbol{M}$, (B 2) has real roots, and all these real roots need to be negative for $\boldsymbol{M}$ to be positive definite. By the Routh–Hurwitz criterion (Barbeau 1989), all roots of (B 2) are negative if and only if

$$\det\boldsymbol{M} > 0, \quad I_2(\boldsymbol{M}) > 0, \quad \begin{vmatrix} I_2(\boldsymbol{M}) & \det\boldsymbol{M} \\ 1 & \mathrm{Tr}\,\boldsymbol{M} \end{vmatrix} > 0,$$

$$\begin{vmatrix} I_2(\boldsymbol{M}) & \det\boldsymbol{M} & 0 \\ 1 & \mathrm{Tr}\,\boldsymbol{M} & I_2(\boldsymbol{M}) \\ 0 & 0 & 1 \end{vmatrix} > 0,$$

or, equivalently,

$$\det\boldsymbol{M} > 0, \qquad I_2(\boldsymbol{M}) > 0, \qquad I_2(\boldsymbol{M}) \cdot \mathrm{Tr}\,\boldsymbol{M} > \det\boldsymbol{M}. \tag{B 3}$$

Using (3.3) and (B 1), we summarize these inequalities as

$$(4|\boldsymbol{S}|^4 - |\boldsymbol{M}|^2)|\boldsymbol{S}|^2 > \det \boldsymbol{M} > 0,$$

where we used the identity $\operatorname{Tr} \boldsymbol{M}^2 = |\boldsymbol{M}|^2$ for the symmetric matrix $\boldsymbol{M}$.

Appendix C

Here we prove statement (i) of Theorem 1. The proof of statement (ii) of the theorem then follows by a reversal of time.

Assume that a trajectory $\boldsymbol{x}(t)$ stays in the hyperbolic region $\mathscr{H}^-(t)$ over the time interval $I = [t_0, t_1]$. Let

$$\dot{\boldsymbol{\xi}} = \boldsymbol{A}(t)\boldsymbol{\xi}, \qquad \operatorname{Tr} \boldsymbol{A}(t) = 0, \tag{C 1}$$

be a linear system whose coefficient matrix $\boldsymbol{A}(t)$ coincides with $\nabla \boldsymbol{v}(\boldsymbol{x}(t), t)$ over the time interval I, and becomes a constant matrix outside a slightly larger time interval

$$I^\epsilon = [t_0 - \epsilon, t_1 + \epsilon] \tag{C 2}$$

for some small constant $\epsilon > 0$. There are infinitely many choices for such an $\boldsymbol{A}(t)$; we shall make our choice more specific below.

We define the rate-of-strain tensor $\boldsymbol{S}(t) = \frac{1}{2}[\boldsymbol{A}(t) + \boldsymbol{A}^T(t)]$ and the strain acceleration tensor

$$\boldsymbol{M}(t) = \frac{\mathrm{d}}{\mathrm{d}t}\boldsymbol{S}(t) + \boldsymbol{S}(t)\boldsymbol{A}(t) + \boldsymbol{A}^T(t)\boldsymbol{S}(t),$$

as well as the zero-strain set

$$Z(t) = \{\boldsymbol{\xi} \mid \langle \boldsymbol{\xi}, \boldsymbol{S}(t)\boldsymbol{\xi} \rangle = 0\}.$$

By assumption, $\boldsymbol{x}(t)$ is in the hyperbolic region $\mathscr{H}^-(t)$ for all $t \in I$. Over this time interval, therefore, $\boldsymbol{S}(t)$ is indefinite with a single negative eigenvalue $s_3(t)$; the set $Z(t)$ is non-empty, and the tensor $\boldsymbol{M}(t)$ is positive definite on $Z(t)$.

We want to select the matrix family $\boldsymbol{A}(t)$ in such a way that the above properties of $\boldsymbol{S}$, Z, and $\boldsymbol{M}$ hold for all times. To this end, we select $\boldsymbol{A}(t)$ so that the function

$$\nu(t) = \min_{\substack{|\boldsymbol{e}(t)|=1 \\ \boldsymbol{e}(t) \in Z(\boldsymbol{x}(t), t)}} \langle \boldsymbol{e}(t), \boldsymbol{M}(\boldsymbol{x}(t), t)\boldsymbol{e}(t) \rangle \tag{C 3}$$

and the single negative eigenvalue, $s_3(t)$, of $\boldsymbol{S}(t)$ satisfy

$$\nu(t) \geqslant \nu_{\min} \overset{\text{def.}}{=} \min_{t \in I} \nu(t) - \epsilon > 0, \qquad s_3(t) \leqslant s_{\max} \overset{\text{def.}}{=} \max_{t \in I} s_3(t) + \epsilon < 0, \qquad t \in \mathbb{R}, \tag{C 4}$$

for small enough $\epsilon > 0$. Then, by the continuity of $\langle \boldsymbol{e}, \boldsymbol{M}\boldsymbol{e} \rangle$ in $\boldsymbol{e}$, for all small enough $\epsilon > 0$, we also have

$$\min_{\substack{|\boldsymbol{e}(t)|=1, \\ \mathrm{dist}\,[\boldsymbol{e}(t), Z(t)] < \epsilon}} \langle \boldsymbol{e}(t), \boldsymbol{M}(t)\boldsymbol{e}(t) \rangle > \frac{\nu_{\min}}{2}. \tag{C 5}$$

For more details on constructing a smooth matrix function $\boldsymbol{A}(t)$ that satisfies (C 3)–(C 5), see Haller (2000).

We shall establish infinite-time Lagrangian hyperbolicity of solutions of the linear system (C 1). From that, we obtain finite-time Lagrangian hyperbolicity for (2.1) while $\boldsymbol{x}(t)$ is in $\mathscr{H}^-(t)$, because (2.1) coincides with (C 1) for $t \in I$.

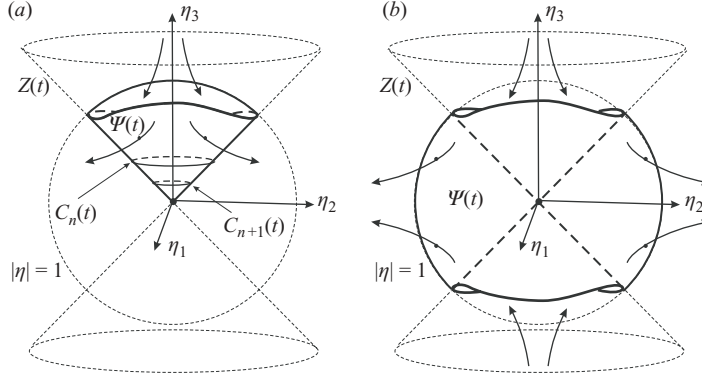*(a) Solutions staying in the cone converge to the origin*

FIGURE 15. The set $\Psi(t)$ for the construction of (a) the stable manifold $E^s(t)$ and (b) the unstable manifold $E^u(t)$.

By (C 4), the quadratic form $V(\boldsymbol{\xi}, t) = \langle \boldsymbol{\xi}, \boldsymbol{S}(t)\boldsymbol{\xi} \rangle$ takes negative values in the interior of the cone $Z(t)$ for all times. Let

$$\Psi(t) = \{ |\boldsymbol{\xi}| \leqslant 1 \mid V(\boldsymbol{\xi}, t) \leqslant 0, \eta_3 \geqslant 0 \}$$

denote the solid half-cone bounded by $Z(t)$ and by the unit sphere, as shown in figure 15(a). While in $\Psi(t)$, any solution $\boldsymbol{\xi}(t)$ of (C 1) approaches the origin monotonically by the estimate

$$\frac{\mathrm{d}}{\mathrm{d}t} |\boldsymbol{\xi}|^2 = 2 \langle \boldsymbol{\xi}, \boldsymbol{S}\boldsymbol{\xi} \rangle = 2V(\boldsymbol{\xi}, t) < 0. \tag{C 6}$$

It remains to show that

$$\lim_{t \to \infty} \boldsymbol{\xi}(t) = 0 \tag{C 7}$$

for any solution $\boldsymbol{\xi}(t)$ that stays in $\Psi(t)$ for all $t \in [t_0, \infty)$. This last statement, however, follows from the same argument given in Haller (2001c) for the two-dimensional case.

(b) *Solutions staying in the cone leave the unit ball in backward time*

In backward time, all solutions starting in $\Psi(t) - \{0\}$ must leave $\Psi(t)$. We obtain this by assuming the contrary for a trajectory $\boldsymbol{\xi}(t)$, and establishing that for such a bounded trajectory,

$$\lim_{t \to -\infty} \mathrm{dist}\, [\boldsymbol{\xi}(t), Z(t)] = 0 \tag{C 8}$$

must hold. This would mean that $Z(t)$ attracts the solution $\boldsymbol{\xi}(t)$ in backward time, whereas $Z(t)$ attracts all nearby solutions in $\Psi(t)$ in forward time. Thus, we conclude that all solutions starting in $\psi(t) - \{0\}$ must leave $\Psi(t)$.

(c) *There exist solutions that stay inside the cone*

Consider an infinite sequence of closed curves $\{C_n(t)\}_{n=1}^{\infty}$ with $C_n(t) \in \Psi(t) \cap Z(t)$, such that each $C_n(t)$ encircles the η_3-axis, and $\lim_{n \to \infty} C_n(t) = 0$, as shown in figure 15(a). In the extended phase space of the $(\boldsymbol{\xi}, t)$ variables, each family of circles, $C_n(\cdot)$, appears as an infinite cylinder,

$$C_n = \{ (\boldsymbol{\xi}, t) \mid \boldsymbol{\xi} \in C_n(t), \ t \in \mathbb{R} \},$$

as shown schematically in figure 16.

There exists a finite time $T_n > 0$ such that at time $t - T_n$, all solutions $(\boldsymbol{\xi}(t), t)$ starting on the cylinder C_n are outside Ψ, forming a deformed cylinder E_n. (The existence of a finite T_n follows from the compactness of $C_n \cap (\mathbb{R}^3 \times I)$, and from the
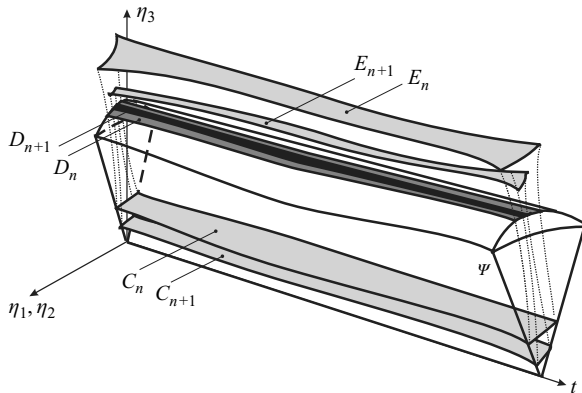
FIGURE 16. The cylinders C_n, D_n, and E_n shown schematically in the four-dimensional space of the $(\boldsymbol{\eta}, t)$ variables.

constancy of $\boldsymbol{A}(t)$ outside the time interval I_ϵ.) All trajectories evolving from C_n into E_n in backward time intersect the boundary of Ψ, delineating another cylinder D_n, as shown in figure 16. Similarly, the cylinder C_{n+1} gives rise to a cylinder $D_{n+1} \subset D_n$ on the boundary of Ψ. By construction, any solution starting from $D_n - D_{n+1}$ exits Ψ somewhere between the circles C_n and C_{n+1}.

The infinite sequence of cylinders, $D_1 \supset D_2 \supset \ldots \supset D_n \supset \ldots$, is a nested sequence of non-empty closed set, and hence

$$D^\infty = \bigcap_{n \geqslant 1} D_n$$

is a non-empty curve by Cantor's theorem. Observe that a point $(\boldsymbol{\xi}^*, t^*) \in D^\infty$ will never exit Ψ because there is no index N for which $(\boldsymbol{\xi}^*, t^*) \in D_N - D_{N+1}$. For any time t^*, therefore, we have found an initial condition $\boldsymbol{\xi}^* \in \Psi$ such that the corresponding solution $\boldsymbol{\xi}^*(t)$ stays in $\Psi(t)$ for all $t > t^*$.

(*d*) *Finite-time stable manifold in the equation of variations*

By (C 7), $\boldsymbol{\xi}^*(t)$ will converge to zero. For a linear system such as (C 1), one initial condition converging to the origin implies the existence of a subspace $E^s(t)$ of initial conditions with the same property. Because $E^s(t)$ must lie entirely inside the cone $Z(t)$, $E^s(t)$ must be a one-dimensional subspace: any two- or three-dimensional subspace would also have points outside $Z(t)$. Furthermore, $E^s(t)$ is a continuously differentiable function of t by the smoothness of solutions of (C 1).

Following the arguments given in Haller (2001*c*), we obtain that for some fixed constant $a > 0$, all solutions $\boldsymbol{\xi}(t)$ with $\boldsymbol{\xi}(t_0) \in E^s(t_0)$ satisfy the decay estimate

$$|\boldsymbol{\xi}(t)| \leqslant |\boldsymbol{\xi}(t_0)| \mathrm{e}^{-a(t-t_0)} \tag{C 9}$$

for any $t, t_0 \in I^\epsilon$.

(*e*) *Finite-time unstable manifold in the equation of variations*

To prove the existence of an unstable manifold for equation (C 1), we now consider the time-dependent set

$$\Psi(t) = \{|\boldsymbol{\xi}| \leqslant 1 \,|\, V(\boldsymbol{\xi}, t) \geqslant 0\},$$

the part of $Z(t)$ and its exterior that lies within the unit sphere (see figure 15*b*). As in section (*a*) above, we obtain that any solution staying in $\Psi(t)$ for all backward times must converge to the origin as $t \to -\infty$.

We now show that there are non-zero solutions of (C 1) that stay in $\Psi(t)$ for all $t \geqslant t_0$. Figure 15(*b*) helps in verifying the following properties of the set

$$\Psi = \{(\boldsymbol{\xi}, t) \,|\, \boldsymbol{\xi} \in \Psi(t), \ t \in \mathbb{R}\}, \tag{C 10}$$

the family of $\Psi(t)$ viewed in space–time:

(i) On the boundary component

$$\partial\Psi^1 = \{(\boldsymbol{\xi}, t) \in \Psi \,|\, |\boldsymbol{\xi}| = 1\} \tag{C 11}$$

of Ψ, the vector field $(\dot{\boldsymbol{\xi}}, \dot{t})$ points strictly inwards in backward time.

(ii) On the boundary component

$$\partial\Psi^2 = \{(\boldsymbol{\xi}, t) \in \Psi \,|\, \boldsymbol{\xi} \in \ Z(t) - \{0\}\} \tag{C 12}$$

of Ψ, the vector field $(\dot{\boldsymbol{\xi}}, \dot{t})$ points strictly outwards in backward time

(iii) The remaining boundary component $\partial\Psi^3 = \partial\Psi - \partial\Psi^1 - \partial\Psi^2$ of Ψ is just the invariant line $\{\boldsymbol{\xi} = 0\}$ in the (ξ, t)-space.

(iv) As a consequence of (i)–(iii), the set of points immediately leaving Ψ in backward time is $W^{im} = \partial\Psi^2$.

(v) Let W^{ev} denote the set of points eventually leaving Ψ in backward time. By definition, $W^{im} \subset W^{ev}$. Because $\partial\Psi^3$ is not in W^{ev}, we conclude that W^{im} is *relatively closed* in W^{ev}, i.e. any Cauchy sequence in W^{im} that does not have a limit in W^{im} will not have a limit in W^{ev} either.

(vi) Ψ is a closed set in the $(\boldsymbol{\xi}, t)$ space.

The properties (iv)–(vi) of Ψ are the defining properties of a backward-time *Wasewsky set* (see Hale 1980). For any Wasewsky set, the *Wasewsky map*

$$\Gamma : W^{ev} \to W^{im}, \tag{C 13}$$

that maps initial conditions in W^{ev} to the point where they leave Ψ in backward time, is continuous.

Suppose that all non-zero solutions leave Ψ eventually in backward time. Then $W^{ev} = \Psi - \partial\Psi^3$, and hence $\Gamma(\Psi - \partial\Psi^3) = \partial\Psi^2$. But a continuous map cannot map the connected set $\Psi - \partial\Psi^3$ into the disconnected set $\partial\Psi^2$, thus we obtain a contradiction. Therefore, there exist solutions that stay in $\Psi(t)$ for all backward times, and these solutions then converge to the $\boldsymbol{\xi} = 0$ solution of (C 1) as $t \to -\infty$. This gives the existence of an unstable manifold $E^u(t)$ for the origin of system (C 1).

The unstable manifold $E^u(t)$ is again a subspace for any fixed t by the linearity of (C 1). It cannot be a one-dimensional subspace, because that would still leave W^{ev} a connected set, thereby violating the continuity of the Wasewsky map (C 13). $E^u(t)$ cannot be three-dimensional either, because that would violate the incompressibility of the linear flow (C 1). Thus $E^u(t)$ must be a two-dimensional subspace for each t, depending continuously on t by the smoothness of solutions of (C 1).

Just as in the case of $E^s(t)$, the above construction gives a finite-time unstable manifold for the linearized flow (2.1). This unstable manifold is not unique, but becomes practically unique if the solution $\boldsymbol{x}(t)$ spends long enough time in the hyperbolic region $\mathscr{H}^-(t)$.

In analogy with (C 9), solutions in $E^u(t)$ obey the growth estimate

$$|\boldsymbol{\xi}(t)| \geqslant |\boldsymbol{\xi}(t_0)| \mathrm{e}^{b(t-t_0)} \tag{C 14}$$

with a positive exponent $b < a$. (This relation between b and a follows from incompressibility.)

(*f*) *Stability of the trajectory* $\boldsymbol{x}(t)$

Under conditions (C 9) and (C 14), Haller (2001*a*) showed the existence of smooth finite-time stable and unstable manifolds $\mathcal{S}(t)$ and $\mathcal{U}(t)$ that are tangent to $E^s(t)$ and $E^u(t)$, respectively, along the trajectory $\boldsymbol{x}(t)$. These manifolds are just the material line and material surface described in statement (i) of Theorem 1.

REFERENCES

BARBEAU, E. J. 1989 *Polynomials*. Springer.

CHONG, M. S., PERRY, A. E. & CANTWELL, B. J. 1990 A general classification of three-dimensional flow field. *Phys. Fluids* A **2**, 765–777.

COTTER, B. A. & RIVLIN, R. S. 1955 Tensors associated with time-dependent stress. *Q. Appl. Maths* **13**, 177–182.

CUCITORE, R., QUADRIO, M. & BARON, A. 1999 On the effectiveness and limitations of local criteria for the identification of a vortex. *Eur. J. Mech.* B/*Fluids* **18**, 261–282.

DOMBRE, T., FRISCH, U., GREENE, J. M., HÉNON, M., MEHR, A. & SOWARD, A. M. 1986 Chaotic streamlines in ABC flows. *J. Fluid Mech.* **167**, 353–391.

ELHMAÏDI, D., PROVENZALE, A. & BABIANO, A. 1993 Elementary topology of two-dimensional turbulence from a Lagrangian viewpoint and single-particle dispersion. *J. Fluid. Mech.* **257**, 533–558.

FRIEDLANDER, S. & VISHIK, M. M. 1991 Instability criteria for the flow of an inviscid incompressible fluid. *Phys. Rev. Lett.* **66**, 2204–2206.

HALE, J. K. 1980 *Ordinary Differential Equations*. Kreiger.

HALLER, G. 2000 Finding finite-time invariant manifolds in two-dimensional velocity fields. *Chaos* **10**, 99–108.

HALLER, G. 2001*a* Distinguished material surfaces and coherent structures in 3D fluid flows. *Physica* D **149**, 248–277.

HALLER, G. 2001*b* Response to "Comment on 'Finding finite-time invariant manifolds in two-dimensional velocity fields'". *Chaos* **11**, 431–437.

HALLER, G. 2001*c* Lagrangian structures and the rate of strain in a partition of two-dimensional turbulence. *Phys. Fluids* **13**, 3365–3385.

HUA, B. L. & KLEIN, P. 1998 An exact criterion for the stirring properties of nearly two-dimensional turbulence. *Physica* D **113**, 98–110.

HUA, B. L., MCWILLIAMS, J. C. & KLEIN, P. 1998 Lagrangian accelerations in geostrophic turbulence. *J. Fluid. Mech.* **366**, 87–108.

HUNT, J. C. R., WRAY, A. & MOIN, P. 1988 Eddies, stream, and convergence zones in turbulent flows. *Center for Turbulence Research Report* CTR-S88.

JEONG, J. & HUSSAIN, F. 1995 On the identification of a vortex. *J. Fluid. Mech.* **285**, 69–94.

KLEIN, P., HUA, B. L. & LAPEYRE, G. 2000 Alignment of tracer gradient vectors in 2D turbulence. *Physica* D **146**, 246–260.

KOH, T. Y. & LEGRAS, B. 2002 Hyperbolic lines and the stratospheric polar vortex. *Chaos* **12**, 382–394.

LAPEYRE, G., HUA, B. L. & LEGRAS, B. 2001 Comment on 'Finding finite-time invariant manifolds in two-dimensional velocity fields'. *Chaos* **11**, 427–430.

LAPEYRE, G., KLEIN, P. & HUA, B. L. 1999 Does the tracer gradient vector align with the strain eigenvectors in 2D turbulence? *Phys. Fluids* **11**, 3729–3737.

LIFSCHITZ, A. 1991 Essential spectrum and local instability condition in hydrodynamics. *Phys. Lett.* A **152**, 199–204.

LUGT, H. J. 1979 The dilemma of defining a vortex. In *Recent Developments in Theoretical and Experimental Fluid Mechanics*. (ed. U. Müller, K. G. Riesner & B. Schmidt), pp. 309–321, Springer.

OKUBO, A. 1970 Horizontal dispersion of floatable trajectories in the vicinity of velocity singularities such as convergencies. *Deep-Sea. Res.* **17**, 445–454.

OTTINO, J. M. 1989 *The Kinematics of Mixing: Stretching, Chaos, and Transport*. Cambridge University Press.

PIERREHUMBERT, R. T. & YANG, H. 1993 Global chaotic mixing on isentropic surfaces. *J. Atmos. Sci.* **50**, 2462–2480.

STONE, H. A., NADIM, A. & STROGATZ, S. H. 1991 Chaotic streamlines inside drops immersed in steady Stokes flows. *J. Fluid Mech.* **232**, 629–646.

TABOR, M. & KLAPPER, I. 1994 Stretching and alignment in chaotic and turbulent flows. *Chaos Soliton Fract.* **4**, 1031–1055.

TRUESDELL, C. A. 1977 *A First Course in rational Continuum Mechanics, Part I: Fundamental Concepts.* Academic.

VERHULST, F. 1990 *Nonlinear Differential Equations and Dynamical Systems.* Springer.

WEISS, J. 1991 The dynamics of enstrophy transfer in 2-dimensional hydrodynamics. *Physica* D **48**, 273–294.